




Blood-brain barrier permeability changes: nonlinear analysis of ECoG based on wavelet and machine learning approaches

Nadezhda Semenova^{1,2,a} , Konstantin Segreev¹, Andrei Slepnev¹, Anastasiya Runnova^{3,1}, Maxim Zhuravlev^{1,3}, Inna Blokhina¹, Alexander Dubrovsky¹, Maria Klimova¹, Andrey Terskov¹, Oxana Semyachkina-Glushkovskaya^{1,4}, Jürgen Kurths^{1,4,5}

¹ Saratov State University, Astrakhanskaya str., 83, Saratov 410012, Russia

² Département d'Optique P. M. Duffieux, Institut FEMTO-ST, Université Bourgogne-Franche-Comté CNRS UMR 6174, Besançon, France

³ State Medical University, B. Kazachaya str., 112, Saratov 410012, Russia

⁴ Physics Department, Humboldt University, Newtonstrasse 15, 12489 Berlin, Germany

⁵ Potsdam Institute for Climate Impact Research, Telegrafenberg A31, 14473 Potsdam, Germany

Received: 12 January 2021 / Accepted: 1 July 2021

© The Author(s), under exclusive licence to Società Italiana di Fisica and Springer-Verlag GmbH Germany, part of Springer Nature 2021

Abstract The blood-brain barrier plays a decisive role in protecting the brain from toxins and pathogens. The ability to analyze the BBB opening (OBBB) is crucial for the treatment of many brain diseases, but it is very difficult to noninvasively monitor OBBB. In this paper we analyze the EEG series of healthy rats in free behaviour and after music-induced OBBB. The research is performed using two completely different methods based on wavelet analysis and machine learning approach. The wavelet-approach demonstrates quantitative changes in the oscillatory structure in EEG signals after music listening, namely, a decrease in the number of patterns to the frequency band $\Delta f[1; 2.5]$ Hz. Using methods of machine learning we analyze the number of fragments of EEG realizations recognized as OBBB. After the music impact the number of recognized OBBB is increased in about 50%. Both methods enable us to recognize OBBB and are in a good agreement with each other. The comparative analysis was carried out using F-measures and ROC-curves.

1 Introduction

The blood-brain barrier (BBB) is a highly selective barrier, which is formed by microvascular endothelial cells surrounded by pericytes and perivascular astroglia. It controls the penetration of blood-borne agents into the brain or the release of metabolites and ions from the brain tissue to blood [1–3]. Therefore, the BBB plays a vital role in protecting the brain against pathogens and toxins. The BBB disruption is associated with aging, dementia, multiple sclerosis, Alzheimer's disease, stroke, brain trauma, infection and tumors [45]. The permeability

^a e-mail: nadya.i.semenova@gmail.com (corresponding author)

of BBB can be varied by neuroendocrine regulation and may play a protective role in injury and stroke [36–39].

The ability to analyze the BBB opening (OBBB) is crucial for the treatment of brain diseases, and it is very difficult to noninvasively monitor OBBB [9,23]. Therefore, there is a strong need to create many safe methods of the assessment of the BBB permeability in clinical practice. There has been substantial progress over the past few years [9,23]. Magnetic resonance tomography (MRI) is an often used technique for the monitoring of OBBB [23]. However, MRI is bulky and cannot be used bedside. The MRI requests the use of contrast agents, which can be even toxic [27,43]. The latter limits its continuous application and usage, especially in the case of children and patients with kidney pathology [13,41]. Therefore, the development of novel promising real-time, bedside, non-invasive, label-free, economically beneficial and readily applicable methods is of highest actual importance, and solving this problem would open a novel era in effective diagnosis and therapy of brain diseases that cause acute and chronic OBBB.

In this paper we consider two different approaches for analysing the OBBB by using electroencephalogram (EEG) time series of healthy rats. The first method is based on the wavelet analysis of EEG signals. This approach is widely used in many biomedical papers [50,54], partially in epilepsy research [4,53], and sleep staging [7,52], which confirms its applicability in these tasks. Nowadays, the wavelet analysis is one of the main tools for processing data in real time and creating brain-computer interface (BCI) devices [12,22,33].

The second method uses a machine learning approach to analyze such EEG signals. Recently, machine learning has been increasingly used in brain activity analysis [11,35,51,56]. The application of machine learning to recognize features of brain activity leads to the use of artificial neural networks (ANNs) of different types and topologies. Basically, ANNs do not analyze the EEG signal in its pure form, but use some characteristics based on the EEGs. For example, power spectral density [44], statistical features [20], wavelet transform [21], combinations of energies of different frequency bands [26] etc. Typically, deep neural networks are used for classification and recognition tasks. As one of examples, the automatic scoring of sleeping stage was recently provided by applying a convolutional neural network [17]. In this work we use deep network with feedforward coupling.

Despite the fact that both methods are based on completely different types of analysis, they show a good ability in recognizing the OBBB. BBB permeability can be evaluated in real time, searching for the EEG signal features, which can be found out by using both wavelet analysis and machine learning approaches.

2 Experiment design and data recording

The experiments were conducted on the same five adult male Wistar-Kyoto rats (250–280 g). All procedures and experiments were done in accordance with the “Guide for the Care and Use of Laboratory Animals” [5]. The experimental protocols were approved by the Local Bioethics Commission of the Humboldt University and the Saratov State University. The animals were kept in a light/dark environment with the lights on from 8:00 to 20:00 and fed ad libitum with standard rodent food and water. The ambient temperature and humidity were maintained at 24.5 ± 0.5 °C and 40–60%, respectively. The general scheme of the experiment is given in Fig. 1.

We use the standard method of electrocorticography (ECoG) in rats during the chronic experiment. At the preliminary stage, we prepared connectors for implantation of epidural ECoG electrodes, combining 2 active electrodes, 1 reference electrode, as well as one

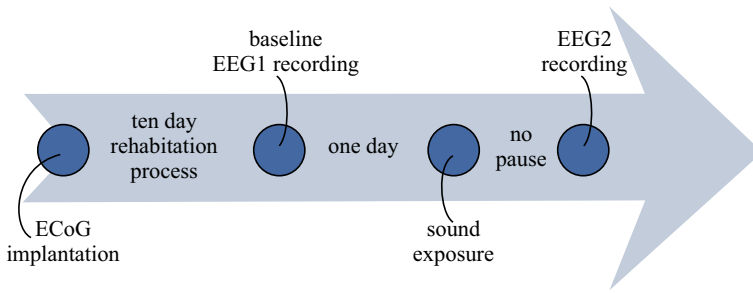


Fig. 1 Key points of the ECoG: study of OBBB induced by the loud music

channel electromyogram (EMG) (Pinnacle Technology, Taiwan) were recorded as follows. The rats were implanted two silver electrodes (tip diameter 2–3 μm) located at a depth of 150 μm in coordinates (L: 2.5 mm and D: 2 mm) from Bregma on either side of the midline under inhalation anesthesia with 2% isoflurane at 1L/min $N_2O/O_2 - 70:30$. The head plate was mounted and small burr holes were drilled. Afterward, ECoG wire leads were then inserted into the burr holes on one side of the midline between the skull and underlying dura. ECoG leads were secured with dental acrylic. An EMG lead was inserted in the neck muscle. Ibuprofen (15 mg/kg) for the relief of postoperative pain was provided in their water supply for two to three days prior to surgery and for three or more days post-surgery. The rats were allowed 10 days to recover from surgery prior to beginning the experiment.

Ten days after surgery, animals were housed individually. The first EEG1-registration was recorded over an hour from 1 to 2 p.m. in free rat behavior. The animal was kept in a tall plexiglass cage (80 \times 40 cm) with an access to water and regular food. The cage is located in a shielded chamber, isolated from an external electromagnetic field.

The day after the baseline EEG1-recording, the rats were underwent to the intermittent music. The detailed description of protocol of music-induced OBBB is described in our early work [48]. To produce the music (70–90–100 dB and 11–10,000 Hz, Scorpions “Still loving you”) we used loudspeaker (ranging of sound intensity 0–130 dB, frequencies 63–15,000 Hz; 100 V, Yerasov Music Corporation, Saint Petersburg, Russia). The repetitive music exposure was performed using the sequence of: 60 s—music on and then 60 s—music off during 2h. The sound level was measured directly in a cage of animals using the sound level meter (Megeon 92130, Russia). Previously, our research group [47,48] have introduced an analysis of the BBB permeability in rats and mice, based on different biophysical methods *in vivo* real time, including fluorescent microscopy of OBBB for Evans Blue (EB) dye (i.v.), real-time two-photon laser scanning microscopy (2PLSM) and MRI. It has been shown, that a discovering the window of music-induced OBBB is possible during 30–60 min after sound exposure [47,48,59]. In this paper, we record again the cortical electrical activity in rats during 60 min (EEG2) after completion of auditory exposure.

Thus, for each of the animals the EEG signals were recorded before and after music-induced OBBB—EEG1 and EEG2, respectively. According to the results of Refs. [47,48], the realization EEG1 was considered as a baseline EEG, and EEG2 corresponded to OBBB. Further, these data were used for the calibration of both methods based on nonlinear and machine learning approaches.

3 Recognition of OBBB using time-frequency analysis

Today, one of the generally accepted nonlinear methods for processing and detecting of oscillatory activity in biomedical signals is continuous wavelet transformation (CWT) [16, 28, 29]. CWT is sufficiently resistant to abrupt changes in the frequency composition of the analyzed experimental signals, which makes it possible to adequately analyze rather short time intervals of highly nonstationary signals. The CWT for an arbitrary real signal $x(t)$ in the general form is defined as follows:

$$W(s, t_0) = \int_{-\infty}^{+\infty} x(t) \psi_{s,t_0}^*(t) dt, \quad (1)$$

where $\psi_{s,t_0}(t)$ is the basic complex function, s is the time scale defining the width of the wavelet, the symbol “*” denotes the complex conjugation. The time scales s of the CWT allow a transition to the classical frequencies f of the Fourier spectrum. Therefore, for convenience and simplicity of the results interpretation, we consider the results in the traditional plane (f, t_0) .

The basic Morlet function $\psi_{s,t_0}(t)$ is often used to analyze the activity of the brain [6, 34]. By analogy with the Fourier power spectrum $F(f)$ for f -frequencies we can estimate the instantaneous frequency distribution of the CWT-energy

$$E(f, t_0) = |W(f, t_0)|^2. \quad (2)$$

CWT allows to analyse an experimental EEG signal $x(t)$ simultaneously in the frequency and time domains. Moreover, the CWT excess property is well known, and is used to search for the fine time-frequency structure of experimental time series, which can be only poorly detected by conventional spectral methods [24, 30–32].

In this paper, we use the CWT “skeleton” method [8, 18, 19, 25, 46] to analyze the oscillatory structure of the EEG. It is based on a simplification of the entire surface $(f; t)$ of the experimental signal $x(t)$ by estimation only the main part of oscillatory activity. Skeletons are the frequency values f_{\max} , defined at each instant of time t_0 . On each coordinate pair $(f_{\max}; t_0)$, the two-dimensional surface CWT—energy E demonstrates an extreme value. For each time t_0 , it is necessary to search for the maxima in the instantaneous CWT spectrum $E(f, t)$ (2):

$$\forall f \in \delta f_{\max}, E(f_{\max}, t_0) \geq E(f, t_0), \quad (3)$$

where $f_{\max} = sc^1$ is the CWT skeleton, δf_{\max} is a δ -region of the f_{\max} frequency component. The first skeleton f_1 is the global maximum in the surface $E(f, t_0)$, i. e. the value of the frequency in the signal spectrum, which correlates with the maximum of the oscillational energy. Next, for each moment of time, we detect a local maxima $sc^1 > sc^2 > \dots > sc^j > \dots > sc^{n_p}$, where n_p is the amount of skeletons.

Further, we limit the consideration of the oscillatory structure in EEG signals to the frequency band $\Delta f[1; 2.5]$ Hz. The choice of this “slow” frequency interval is due to the evidence in the literature on the presence of biomarkers in brain slow activity reflecting the BBB permeability changes [40, 51]. Thus, at each time moment t_0 we estimate which skeleton’s number N_0 falls into a certain frequency range Δf . And next we calculate the average number of $N(t)$ skeletons falling into the band Δf over the time interval $\Delta t = 50$ sec.

In Fig. 2a the results of estimating the number of $N(t)$ skeletons for one experimental animal are presented. We observe that the number of patterns in the low frequency range Δf_1 increases after a powerful auditory impact (EEG2). After evaluating the distribution of

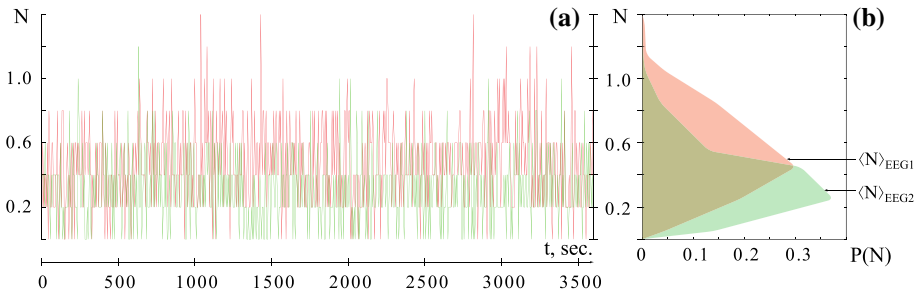


Fig. 2 Results of evaluating the wavelet-based characteristics for animal #3. **a** Time-dependence of the N average number of CWT-skeletons in the frequency range $\Delta f_1 [1; 2.5]$ Hz. The red line is the calculation result for EEG1, the green line corresponds to the characteristic for EEG2. **b** The probability distributions of N skeletons. Red color shows the distribution for EEG1 (no influence on the BBB-permeability), and green—for EEG2 (after auditory impact). The arrows indicate the mean values for each distribution

the number of patterns for records EEG1 and EEG2, their mean values differ $\langle N \rangle_{EEG1} \neq \langle N \rangle_{EEG2}$ (see Fig. 2b). A similar situation is observed in the slow oscillatory activity of the EEG for all experimental animals. Next, we use the detectable value $\langle N \rangle_{EEG2}$ as the threshold value that characterizes the moment of BBB permeability changes.

For each experimental animal, individual threshold values were obtained $\langle N \rangle_{EEG2} = \{0, 31863; 0, 45614; 0, 462575; 0, 485995; 0, 52011\}$. Thus, we estimated the EEG-dynamics of the brain activity based on the $N(t)$ -dynamic. Generally, the value of dependence $N(t)$ in EEG2-record exceeded the threshold $\langle N \rangle_{EEG2}$ throughout first third of the recording. Next, this value $N(t)$ irregularly reduced towards the end of the EEG2-record, when, apparently, the influence of the sound impact was compensated by the neurophysiological system, and the BBB-permeability returned to its usual value. Based on this, we assumed that the excess of the $N(t)$ patterns number of the $\langle N \rangle_{EEG2}$ threshold value correlated with an increase in the BBB permeability. So, when the corresponding threshold value $N(t) \geq \langle N \rangle_{EEG2}$ is exceeded, we assumed that the permeability of the BBB was increased.

4 ANN based method

In order to estimate the permeability of the BBB, a deep neural network is used. The training set is prepared using standard Python tools (TensorFlow, NumPy, pandas, etc.) The network is constructed and trained using an open-source deep learning API Keras [10]. The use of EEG signals in their pure form is a non-trivial task for the ANN, since it requires a large number of neurons and layers. This dimension problem can be solved by specially prepared statistical characteristics calculated from these EEGs. There is a number of papers on sleep recognition, in which the EEG signals were not used by ANN, but their averages, variations and deviations from the mean [20,21,26,44,58]. After comparing several commonly used statistical characteristics, we found that the relative standard deviation is the most effective for our problem. This characteristic can also be interpreted as a signal-to-noise ratio (SNR) [14], and calculated as the ratio between the mean of the signal $\mu(\cdot)$ and its standard deviation $\sigma(\cdot)$:

$$SNR(x) = \frac{\mu(x)}{\sigma(x)}. \tag{4}$$

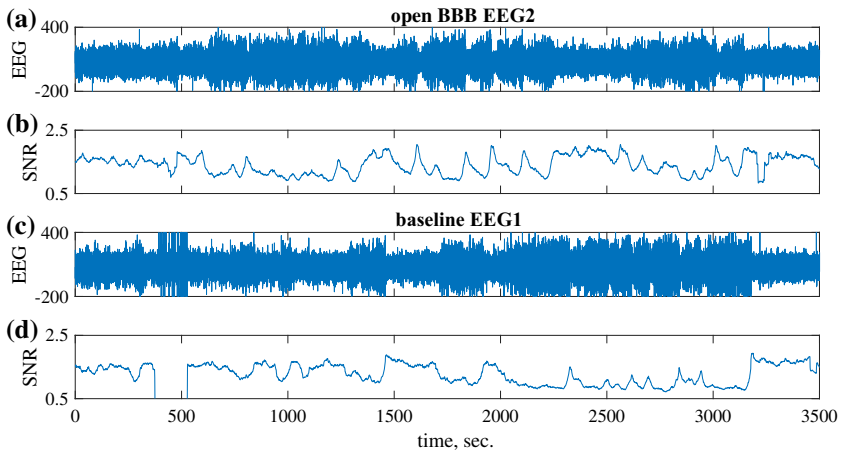


Fig. 3 Examples of EEG signals (a, c) for animal #1 and corresponding SNR characteristics (Eq. 4) shown in panels (b, d)

Each point of this characteristic is prepared for some averaging window. The window size is fixed to 30 s. In order to make the SNR realization smoother, the calculations were performed with a slowly shifting time window with a 1-s step. This leads to a new temporal determination of SNR with a time step of 1 s, where each point corresponds to the SNR value obtained from a thirty-second window of EEG data. Figure 3 shows the EEG of one of the animals (panels a, c) and the calculated SNR characteristics (panels b, d).

To get the training SNR examples, we used EEG signals before (EEG1) and after (EEG2) artificially increased permeability of the BBB [49]. During the training, the fragments of SNR for the rat after music stimulation were marked as the expected response “1” (i.e. BBB is open), while fragments of rats before this stimulation corresponded to the response “0” (i.e. baseline BBB). Thus, the ANN response to an unknown signal can be interpreted as a degree of the averaged “permeability” of BBB over the considered time period.

The input layer of our ANN consists of 90 neurons. Each time the network receives a 90-s SNR realization as an input. A smaller number of input neurons leads to slower training and a sharp jump into overtraining. A larger number leads to inaccuracies in the temporal marking, since it gives the response delay of more than 1.5 min. Also a few deep ANN configurations with constant numbers of neurons in the hidden layers 200, 500, 1000 have been considered. A network with a variable number of neurons in hidden layers ($500 \times 200 \times 500 \times 200$) has shown the optimal results during training and testing. The network scheme and the training process are shown in Fig. 4. Panel (b) shows the general dependency of accuracy on training epochs for training and cross-validation data. Next, we stop the training process when the accuracy for both sets becomes equal, or when the accuracy for cross-validation data becomes about 70%. All the layers have the sigmoid activation function $f(x) = 1/(1 + e^{-x})$.

To process the data of each rat, the network was trained on the data of the other rats. This method is also known as leave-one-subject-out cross validation, and is often used to increase the number of training and testing implementations. Each EEG recording was done using two channels. The SNR and ANN markup were prepared for both signals separately. To increase the accuracy, the network responses for both channels were multiplied. Thus, if the network recognises the inputs from both channels are recognized simultaneously as “1” (BBB is open), then the final answer is “1”. If one channel leads to the answer “0” and the

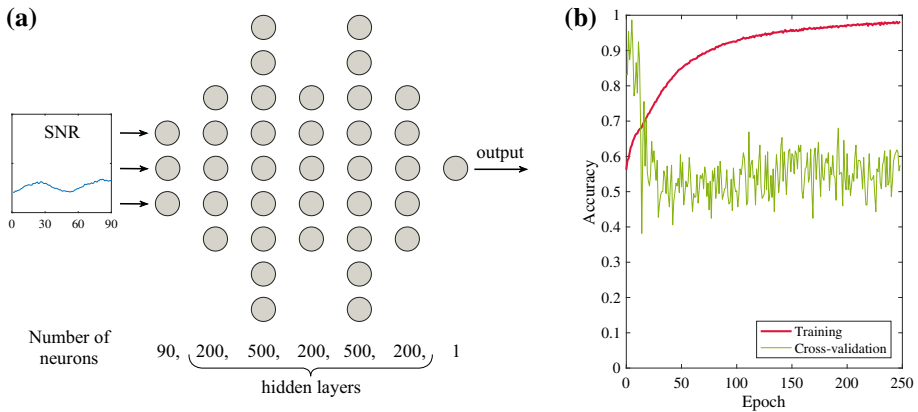


Fig. 4 Schematic diagram of considered ANN (a) and the dynamics of accuracy during training depending on the epoch number (b)

second one leads to the answer “1”, then the final response is “0”. Since the network produces a real number from 0 to 1, the multiplication of responses from two channels can lead to an increase in intermediate values. To eliminate this, the threshold 0.5 has been introduced. Since then, the answers $y \geq 0.5$ are regarded as “1” (BBB is open), while responses $y < 0.5$ complies with “0” (baseline BBB). Figure 5 shows a temporal evolution of ANN responses for an animal with artificially open barrier, whose signals have been shown in Fig. 3(a,b). The gray line represents the result of multiplying the signals from both channels, and red points represent the final answer with the threshold 0.5.

The ANN found 32% of the data similar to the open barrier for implementations after music-induced OBBB. In the case of free behaviour, this percentage was 24%. These ratios are averaged over all considered animals. In order to exclude the peculiarities of the training, the networks have been trained 5 times for each animal with an accuracy of at least 96% (approximately 250 epochs). Figure 6 shows the examples of SNR obtained using fragments of EEG signals recognized as signals with open BBB (top panels) and baseline BBB (bottom panels).

5 Comparison of two independent methods of data processing

Figure 5 shows the intersection of both methods from Sects. 3 and 4 by green background color. We find that both methods are in a good agreement with each other. To test this numerically, we calculate the so-called F-measure [55], which is often used for statistical analysis of binary classification. It is the harmonic mean between precision and recall. The precision is the number of correctly identified positive results divided by the number of all positive results, including those not identified correctly, and the recall is the number of correctly identified positive results divided by the number of all samples that should have been identified as positive. For such an assessment, one can choose one of the methods as true, for example, the wavelet method, and then count the number of matches of both methods for the answer “yes” (true-positive, TP), the number of matches for the answer “no” (true-negative, TN), as well as mismatches (false-positive, FP, and false-negative, FN). Based on this, the

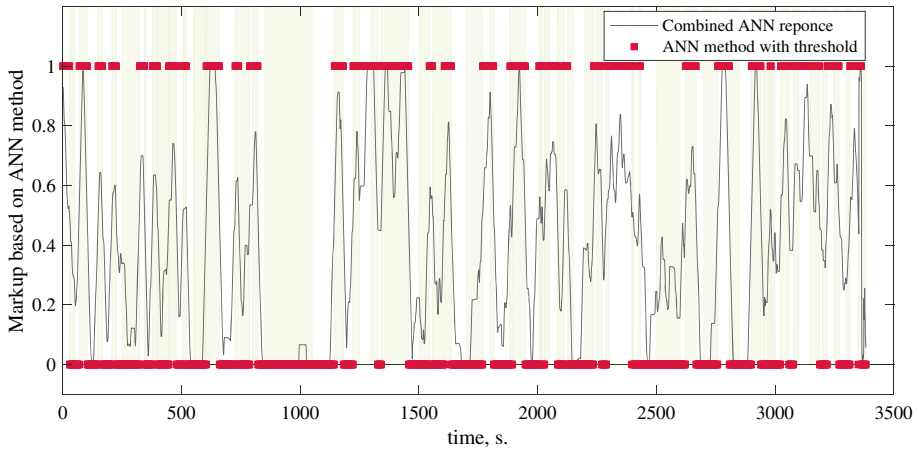


Fig. 5 Temporal evolution of ANN responses for animal #1 after music-induced OBBB. The multiplication of network responses for both EEG channels is shown in gray. Red points correspond to the binary classification after introducing the threshold 0.5. Green areas show time intervals in which both markings coincide: (1) based on ANN answers and (2) wavelet method from Sect. 3

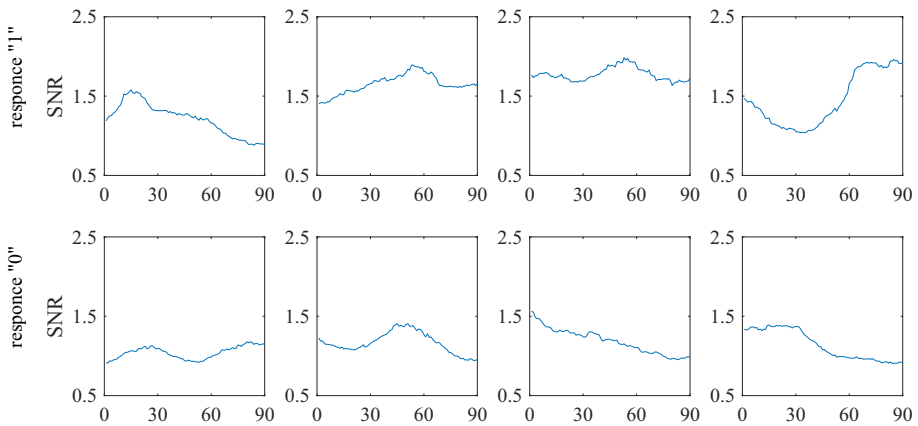


Fig. 6 Examples of input SNR implementations on which the neural network exhibited a similarity to OBBB (top panels) and baseline BBB (bottom panels)

F-measure is calculated as follows:

$$P = \frac{TP}{TP + FP}, R = \frac{TP}{TP + FN}, F^+ = 2 \frac{PR}{P + R} \quad (5)$$

Thus, the F-measure F^+ is an evaluation of the correctness for the answers “yes”. If we replace all letters “P” by “N” in Eq. (5), and vice versa, then this will be an estimate of the correctness for the answer “no”, which we denote as F^- . Table 1 shows the percentage of fragments recognized as OBBB for one animal after 5 trainings. Afterward, the general percentage of fragments, recognized as OBBB, has been averaged over all animals and over all five trainings. Table 1 also contains the results of calculating the F-measure for five ANN trainings, as well as the averaged characteristics. Thus, according to the calculations of the F-measure, we can conclude that the intersection of 35% in the answers that the barrier is

Table 1 Percentage of fragments recognized as OBBB and not, and F-measures of animal #1 for five ANN trainings on fragments of the other animals

| Training: | Tr.1 | Tr.2 | Tr.3 | Tr.4 | Tr.5 | Averaged |
|---|------|------|------|------|------|----------|
| % of open barrier in realization with an open barrier | 35 | 22 | 21 | 38 | 27 | 28.5 |
| % of open barrier in realization with free behaviour | 24 | 18 | 13 | 24 | 20 | 19.8 |
| F-measure on responses “BBB is open”, F^+ | 0.38 | 0.35 | 0.32 | 0.38 | 0.34 | 0.35 |
| F-measure on responses “BBB is closed”, F^- | 0.73 | 0.77 | 0.79 | 0.72 | 0.75 | 0.75 |

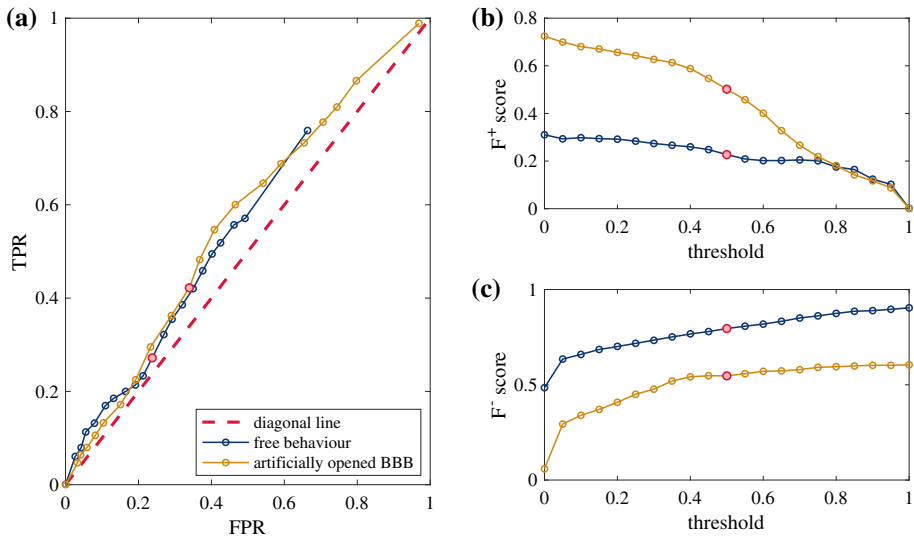


Fig. 7 Statistical comparison of both methods using ROC-curve (a), and F-scores (Eq. 5) for positive (b) and negative (c) responses

open, and 75% in the answers about the baseline barrier. These values, averaged over all animals, are 28% and 70%.

Another measure that allows one to assess the quality of the classification is the receiver operating characteristic (ROC-curve). The ROC curve is created by plotting the true positive rate ($TPR = \frac{TP}{TP+FN}$) against the false positive rate ($FPR = \frac{FP}{FP+TN}$) at various threshold settings [15,42]. The classifier is considered to be good if the ROC-curve is above the diagonal (see Fig. 7). However, the degree of success of the classifier is roughly estimated by how far this curve is above the diagonal, and, accordingly, how large is the area below it. Figure 7 shows the ROC curves for different threshold values in cases of artificially opened BBB (orange color) and free behaviour (blue color), when the rat can either sleep or be awake. The markings obtained by the method, described in Sect. 3, were used as a verification data. Both curves are above the diagonal, which indicates the similarity of the methods. In addition, the figure shows the results of calculating the F-measures for both implementations with variation of the threshold parameter. The points corresponding to the 0.5 threshold are highlighted by red. As follows from the graphs of F-measures, the threshold 0.5 is optimal for positive and negative answers. An increase in the threshold leads to an increase in false positives, and a decrease leads to a loss of sensitivity when the network says that it is the baseline BBB.

6 Conclusions

This work is devoted to the investigation of sustained changes in brain activity after music-induced OBBB. BBB permeability is analyzed using two different methods—wavelet estimation of the oscillatory characteristics of the EEG and machine learning using SNR characteristics. The wavelet analysis demonstrated an increase in the number of arising oscillations in the low-frequency region (1–2.5 Hz), which is universal for all animals. However, the threshold for the increase in oscillatory activity in these frequencies is highly individual for each animal.

The second method is based on the search of special features of SNR realisation which are common for animals with OBBB. The use of a machine learning approach allows us to demonstrate a high level of universality of the revealed “portrait” of the electrical activity of the brain after an artificial increase in the permeability of the BBB.

Despite the fact that both methods are based on different characteristics, they show a good overlap both for animals with artificially open BBB and for animals in free behaviour without any influences. Quantification of the methods agreement was based on ROC curves and F-measures of positive and negative responses. Both methods recognized a non-zero probability of opening the barrier for animals with normal behaviour. It is possible that this effect is related to the constancy of brain activity patterns during the physiological state of sleep. A number of authors have linked spontaneous changes in BBB permeability to certain stages of sleep, promoting a repair and clearance of brain tissue [40,47,59].

Analysis of EEG activity characteristics after sound exposure, that probably are the markers of increased BBB permeability, demonstrates the presence of a pronounced window of 15–20 mins demonstrated by both methods. After that, the EEG characteristics return to the level of baseline ECoG. At the same time, after 5–10 min, the EEG again demonstrates an increase in these characteristics. This probably corresponds to the features of “soft” reversible increase in the BBB permeability, arising as a result of music exposure. At the same time, for example, anesthesia BBB permeability impair, apparently, has a fundamentally different physiological mechanism of its disruption, leading to a catastrophic dysfunction [57].

In the future, we plan to increase of the experimental groups and to include instrumental methods of optical control of the BBB permeability. The preliminary analysis of brain activity during the sleeping state of the animals is of our interest. Probably, some sleep stages would be accompanied with the brain activity, similar to the results of music-induced OBBB.

Acknowledgements This work has been supported by the RF Government Grant No. 075-15-2019-1885 in part of the biological interpretation and machine learning approach. In the part of the development of numeric method of data analysis this work has been supported by the Council for Grants of the President of the Russian Federation for the State Support of Young Russian Scientists (Project No. MD-645.2020.9). The biological experiment has been partially supported by Russian Science Foundation Grant No. 18-75-10033.

References

1. N. Abbott, Dynamics of cns barriers: evolution, differentiation, and modulation. *Cell. Mol. Neurobiol.* **25**, 5–23 (2005)
2. N. Abbott, A.A. Patabendige, D.E. Dolman, S. Yusof, D. Begley, Structure and function of the blood-brain barrier. *Neurobiol. Dis.* **37**, 13–25 (2010)
3. N. Abbott, L. Rönnbäck, L. Hansson, Astrocyte-endothelial interactions at the blood-brain barrier. *Nat. Rev. Neurosci.* **7**, 41–53 (2006)
4. H. Adeli, Z. Zhou, N. Dadmeh, Analysis of EEG records in an epileptic patient using wavelet transform. *J. Neurosci. Methods* **123**(1), 69–87 (2003). [https://doi.org/10.1016/s0165-0270\(02\)00340-0](https://doi.org/10.1016/s0165-0270(02)00340-0)

5. U. Albus, Guide for the care and use of laboratory animals (8th edn). Lab. Anim. **46**, 267–268 (2012)
6. A. Aouinet, C. Adnane, Electrocardiogram denoised signal by discrete wavelet transform and continuous wavelet transform. Signal Process. Int. J. **8**(1), 1 (2014)
7. V. Bajaj, R. Pachori, Automatic classification of sleep stages based on the time-frequency image of eeg signals. Comput. Methods Programs Biomed. **112**(3), 320–328 (2013)
8. P. Cavalier, D. O'Hagan, Maximum wavelet coefficient points for potential field analysis and inversion. In: International conference on engineering geophysics, Al Ain, United Arab Emirates, 9–12 October 2017, pp. 128–131. Society of Exploration Geophysicists (2017)
9. Y. Chassidim, R. Veksler, S. Lublinsky, G. Pell, A. Friedman, I. Shelef, Quantitative imaging assessment of blood-brain barrier permeability in humans. Fluids Barriers CNS **10**(1), 9 (2013)
10. F. Chollet et al. Keras. GitHub (2015). <https://github.com/fchollet/keras>
11. C. Davatzikos, K. Ruparel, Y. Fan, D. Shen, M. Acharyya, J. Loughhead, R. Gur, D. Langleben, Classifying spatial patterns of brain activity with machine learning methods: application to lie detection. NeuroImage **28**(3), 663–668 (2005) <https://doi.org/10.1016/j.neuroimage.2005.08.009>. <http://www.sciencedirect.com/science/article/pii/S1053811905005914>
12. E.C. Djamel, R.D. Putra, Brain-computer interface of focus and motor imagery using wavelet and recurrent neural networks. TELKOMNIKA Telecommun. Comput. Electron. Control **18**(4), 2748–2756 (2020)
13. I. Elbeshlawi, M.S. AbdelBaki, Safety of gadolinium administration in children. Pediatr. Neurol. **86**, 27–32 (2018)
14. B. Everitt, *The Cambridge dictionary of statistics* (Cambridge University Press, Cambridge, 1998)
15. T. Fawcett, An introduction to roc analysis. Pattern Recogn. Lett. **27**, 861–874 (2006)
16. Q. Feng, M. Zhang, Y. Zhang, N. Jiang, J. Zhang, Multi-scale representation of sleep electroencephalogram events for healthy adult using wavelet transformation. J. Med. Imaging Health Inf. **7**(5), 928–933 (2017)
17. E. Fernandez-Blanco, D. Rivero, A. Pazos, Eeg signal processing with separable convolutional neural network for automatic scoring of sleeping stage. Neurocomputing **410**, 220–228 (2020)
18. V. Grubov, V. Musatov, V. Maksimenko, A. Pisarchik, A. Runnova, A. Hramov, Development of intelligent system for classification of multiple human brain states corresponding to different real and imaginary movements. Cybern. Phys. **6**, 103–107 (2017)
19. V. Grubov, A. Runnova, M. Zhuravlev, V. Maksimenko, S. Pchelintseva, A. Pisarchik, Perception of multistable images: Eeg studies. Cybern. Phys. **6**, 108–113 (2017)
20. A. Hassan, S. Bashar, M. Bhuiyan, On the classification of sleep states by means of statistical and spectral features from single channel electroencephalogram. In: International conference on advances in computing, communications and informatics (ICACCI), pp. 2238–2243 (2015)
21. A. Hassan, M. Bhuiyan, Automated identification of sleep states from EEG signals by means of ensemble empirical mode decomposition and random under sampling boosting. Comput. Methods Prog. Biomed. **140**, 201–210 (2017). <https://doi.org/10.1016/j.cmpb.2016.12.015>
22. I.T. Hettiarachchi, T.T. Nguyen, S. Nahavandi, Motor imagery data classification for bci application using wavelet packet feature extraction. In: International Conference on Neural Information Processing, pp. 519–526. Springer (2014)
23. A.K. Heye, R.D. Culling, M.C. Valdés Hernández, M.J. Thrippleton, J.M. Wardlaw, Assessment of blood-brain barrier disruption using dynamic contrast-enhanced MRI: a systematic review. NeuroImage Clin **6**, 262–274 (2014)
24. A.E. Hramov, A.A. Koronovskii, V.A. Makarov, A.N. Pavlov, E. Sitnikova, *Wavelets in neuroscience* (Springer, New York, 2015)
25. A.E. Hramov, V.A. Maksimenko, S.V. Pchelintseva, A.E. Runnova, V.V. Grubov, V.Y. Musatov, M.O. Zhuravlev, A.A. Koronovskii, A.N. Pisarchik, Classifying the perceptual interpretations of a bistable image using eeg and artificial neural networks. Front. Neurosci. **11**, 674 (2017)
26. Y.L. Hsu, Y.T. Yang, J.S. Wang, C.Y. Hsu, Automatic sleep stage recurrent neural classifier using energy features of eeg signals. Neurocomputing **104**, 105–114 (2013)
27. M. Kaller, J. An, *Contrast agent toxicity* (StatPearls Publishing, Treasure Island, 2020)
28. S.K. Khare, V. Bajaj, S. Siuly, G. Sinha, Classification of schizophrenia patients through empirical wavelet-transformation using electroencephalogram signals. In *Modelling and Analysis of Active Biopotential Signals in Healthcare*, (IOP publishing, 2020), pp. 1–1–26. <https://doi.org/10.1088/978-0-7503-3279-8ch1>
29. J.P. Lachaux et al., Estimating the time-course of coherence between single-trial brain signals: an introduction to wavelet coherence. Neurophysiol. Clin. **32**(3), 157–174 (2002)
30. V.A. Maksimenko, A.E. Runnova, N.S. Frolov, V.V. Makarov, V. Nedaivozov, A.A. Koronovskii, A. Pisarchik, A.E. Hramov, Multiscale neural connectivity during human sensory processing in the brain. Phys. Rev. E **97**(5), 052405 (2018)

31. V.A. Maksimenko, A.E. Runnova, M.O. Zhuravlev, P. Protasov, R. Kulanin, M.V. Khranova, A.N. Pisarchik, A.E. Hramov, Human personality reflects spatio-temporal and time-frequency eeg structure. *PLoS one* **13**(9), e0197642 (2018)
32. L. Montefusco, *Wavelets* (Elsevier Science, Amsterdam, 2014)
33. T. Nguyen, A. Khosravi, D. Creighton, S. Nahavandi, Eeg signal classification for bci applications by wavelets and interval type-2 fuzzy logic systems. *Expert Syst. Appl.* **42**(9), 4370–4380 (2015)
34. A. Ovchinnikov, A. Hramov, A. Lutjehann, A. Koronovskii, G. van Luijckelaar, Method for diagnostics of characteristic patterns of observable time series and its real-time experimental implementation for neurophysiological signals. *Tech. Phys.* **56**(1), 1–7 (2011)
35. R. Palaniappan, D.P. Mandic, Biometrics from brain electrical activity: A machine learning approach. *IEEE Trans. Pattern Anal. Mach. Intell.* **29**(4), 738–742 (2007)
36. W. Pan, W. Banks, A. Kastin, Blood-brain barrier permeability to ebitatide and tnf in acute spinal cord injury. *Exp. Neurol.* **146**, 367–373 (1997)
37. W. Pan, Y. Ding, Y. Yu, H. Ohtaki, T. Nakamachi, A. Kastin, Stroke upregulates tnf alpha transport across the blood-brain barrier. *Exp. Neurol.* **198**, 222–233 (2006)
38. W. Pan, A. Kastin, R. Bell, R. Olson, Upregulation of tumor necrosis factor a transport across the blood-brain barrier after acute compressive spinal cord injury. *J. Neurosci.* **19**, 3649–3655 (1999)
39. W. Pan, A. Kastin, L. Gera, J. Stewart, Bradykinin antagonist decreases early disruption of the blood-spinal cord barrier after spinal cord injury in mice. *Neurosci. Lett.* **307**, 25–28 (2001)
40. A. Pavlov, A. Dubrovsky, A. Koronovskii Jr., O. Pavlova, O. Semyachkina-Glushkovskaya, J. Kurths, Extended detrended fluctuation analysis of sound-induced changes in brain electrical activity. *Chaos Soliton Fract.* **139**, 109989 (2020)
41. M.A. Perazella, Gadolinium-contrast toxicity in patients with kidney disease: nephrotoxicity and nephrogenic systemic fibrosis. *Curr. Drug. Saf.* **3**, 67–75 (2008)
42. D.M.W. Powers, Evaluation: From precision, recall and f-factor to roc, informedness, markedness & correlation. *J. Mach. Learn. Technol.* **2**(1), 37–63 (2011)
43. M. Rogosnitzky, S. Branch, Gadolinium-based contrast agent toxicity: a review of known and proposed mechanisms. *Biometals* **29**(365–376) (2016)
44. M. Ronzhina, O. Janousek, J. Kolarova, M. Novakova, P. Honzik, I. Provaznik, Sleep scoring using artificial neural networks. *Sleep Med. Rev.* **16**, 251–263 (2012)
45. G. Rosenberg, Neurological diseases in relation to the blood-brain barrier. *J. Cereb. Blood Flow Metab.* **32**, 1139–1151 (2012)
46. A.E. Runnova, M.O. Zhuravlev, A.N. Pysarchik, M.V. Khranova, V.V. Grubov, The study of cognitive processes in the brain eeg during the perception of bistable images using wavelet skeleton. In: *Dynamics and Fluctuations in Biomedical Photonics XIV*, vol. 10063, p. 1006319. International Society for Optics and Photonics (2017)
47. O. Semyachkina-Glushkovskaya, A. Abdurashitov, A. Dubrovsky, D. Bragin, O. Bragina, N. Shushunova, G. Maslyakova, N. Navolokin, A. Bucharskaya, V. Tuchind et al., Application of optical coherence tomography for in vivo monitoring of the meningeal lymphatic vessels during opening of blood-brain barrier: mechanisms of brain clearing. *J. Biomed. Opt.* **22**(12), 121719 (2017)
48. O. Semyachkina-Glushkovskaya, A. Esmat, D. Bragin, O. Bragina, A.A. Shirokov, N. Navolokin, Y. Yang, A. Abdurashitov, A. Khorovodov, A. Terskov, M. Klimova, A. Mamedova, I. Fedosov, V. Tuchin, J. Kurths, Phenomenon of music-induced opening of the blood-brain barrier in healthy mice. *bioRxiv* p. 2020.10.03.324699 (2020). <https://doi.org/10.1101/2020.10.03.324699>. <https://app.dimensions.ai/details/publication/pub.1131448754> and <https://www.biorxiv.org/content/biorxiv/early/2020/10/05/2020.10.03.324699.full.pdf>
49. O. Semyachkina-Glushkovskaya, A. Esmat, D. Bragin, O. Bragina, A.A. Shirokov, N. Navolokin, Y. Yang, A. Abdurashitov, A. Khorovodov, A. Terskov, M. Klimova, A. Mamedova, I. Fedosov, V. Tuchin, J. Kurths, Phenomenon of music-induced opening of the blood-brain barrier in healthy mice. *Proc. Roy. Soc. B Biol. Sci.* **287**(1941), 20202337 (2020). <https://doi.org/10.1098/rspb.2020.2337>. <https://royalsocietypublishing.org/doi/abs/10.1098/rspb.2020.2337>
50. A. Subasi, Eeg signal classification using wavelet feature extraction and a mixture of expert mode. *Expert Syst. Appl.* **32**, 1084–1093 (2007)
51. Z. yao Tian, L. Qian, L. Fang, X. hua Peng, X. hu Zhu, M. Wu, W. zhi Wang, W. han Zhang, B. qi Zhu, M. Wan, X. Hu, J. Shao, Frequency-specific changes of resting brain activity in parkinson's disease: a machine learning approach. *Neuroscience* **436**, 170–183 (2020). <https://doi.org/10.1016/j.neuroscience.2020.01.049>. <http://www.sciencedirect.com/science/article/pii/S0306452220300798>
52. R. Tripathy, S. Ghosh, P. Gajbhiye, U. Acharya, Development of automated sleep stage classification system using multivariate projection-based fixed boundary empirical wavelet transform and entropy features extracted from multichannel eeg signals. *Entropy* **22**(1141) (2020)

53. A. Tzallas, M. Tsipouras, D. Fotiadis, Epileptic seizure detection in EEGs using time-frequency analysis. *IEEE Trans. Inf. Technol. Biomed.* **13**(5), 703–710 (2009)
54. M. Unser, A. Aldroubi, A review of wavelets in biomedical applications. *Proc. IEEE* **84**(4), 626–638 (1996)
55. C.J. Van Rijsbergen, *Information Retrieval* (University of Glasgow, Information Retrieval Group, 1979)
56. J. Wei, T. Chen, C. Li, G. Liu, J. Qiu, D. Wei, Eyes-open and eyes-closed resting states with opposite brain activity in sensorimotor and occipital regions: Multidimensional evidences from machine learning perspective. *Front. Human Neurosci.* **12**, 422 (2018) <https://doi.org/10.3389/fnhum.2018.00422>. <https://www.frontiersin.org/article/10.3389/fnhum.2018.00422>
57. S. Yang, C. Gu, E.T. Mandeville, Y. Dong, E. Esposito, Y. Zhang, G. Yang, Y. Shen, X. Fu, E.H. Lo et al., Anesthesia and surgery impair blood-brain barrier and cognitive function in mice. *Front. Immunol.* **8**, 902 (2017)
58. G. Zhu, Y. Li, P. Wen, Analysis and classification of sleep stages based on difference visibility graphs from a single-channel eeg signal. *IEEE J. Biomed. Health Inf.* **18**(6), 1813–1821 (2014)
59. E. Zinchenko, N. Navolokin, A. Shirokov, B. Khlebtsov, A. Dubrovsky, E. Saranceva, A. Abdurashitov, A. Khorovodov, A. Terskov, A. Mamedova et al., Pilot study of transcranial photobiomodulation of lymphatic clearance of beta-amyloid from the mouse brain: breakthrough strategies for non-pharmacologic therapy of alzheimer's disease. *Biomed. Opt. Exp.* **10**(8), 4003–4017 (2019)